Langmuir

Article

pubs.acs.org/Langmuir

Polyfuran-Derived Microporous Carbons for Enhanced Adsorption of CO_2 and CH_4

Jun Wang,[†] Rajamani Krishna,[‡] Xiaofei Wu,[†] Yingqiang Sun,[†] and Shuguang Deng*[,†]

[†]Chemical & Materials Engineering Department, New Mexico State University, Las Cruces, New Mexico 88003, United States

[‡]van't Hoff Institute for Molecular Sciences, University of Amsterdam, Science Park 904, 1098 XH Amsterdam, The Netherlands

Supporting Information

ABSTRACT: Oxygen-doped microporous carbons were synthesized by chemical activation of polyfuran with KOH or $ZnCl_2$ at 600 and 800 °C. It was found that KOH preserves and $ZnCl_2$ eliminates the O−C functional groups in the activation process. The O-doped carbon activated with KOH at 800 °C exhibited a high CO_2 capacity (4.96 mmol g^{-1}, 273 K, 1 bar) and CH_4 adsorption capacity (2.27 mmol g^{-1}, 273 K, 1 bar). At 298 K and 1 bar, a very high selectivity for separating CO_2/N_2 (41.7) and CO_2/CH_4 (6.8) gas mixture pairs was obtained on the O-doped carbon activated with KOH at 600 °C. The excellent separation ability of the O-doped carbons was demonstrated in transient breakthrough simulations of $CO_2/CH_4/N_2$ mixtures in a fixed bed adsorber. The isosteric adsorption heats of the O-doped carbons were also significantly lower than those of MOF-74 and NaX zeolite. The O-doped microporous carbon adsorbents appear to be a very promising adsorbent for CO_2 capture from flue gas, biogas upgrading, and CH_4 storage.

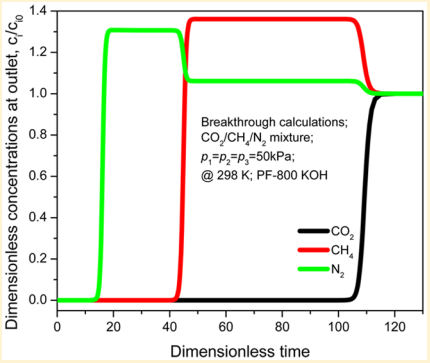

1. INTRODUCTION

Global warming has become one of the most concerned problems due to the overwhelming emission of greenhouse gases (i.e., carbon dioxide, methane, nitrogen dioxide, etc.).[1−3] Aqueous ammonia[4] is widely used for capturing CO_2 from flue gases because it is a very efficient solvent for absorbing CO_2. However, it requires lots of energy to regenerate the absorbents, resulting in a net increasing CO_2 level in the atmosphere. Therefore, finding new generation of adsorbents for capturing CO_2 from flue gas is critical to mitigate the global warming problem. Methane is a biorenewable energy source that may help us to alleviate fossil fuel dependence. However, storage, purification, and transportation are still main problems for large scale-up applications of low grade biogas that is generated in aerobatic digestion of biomass. Polymer-based activated adsorbents could be very promising in those applications because of easy manufacturing, high CO_2 adsorption capacity, high separation selectivity, easy to regenerate, and stability.[1,5,6]

Many different adsorbents have been studied for capturing CO_2 from flue gas, such as zeolites,[7] metal−organic frameworks (MOFs),[8] polymers of intrinsic microporosity (PIMs),[9,10] hyper-cross-linked polymers (HCPs),[11,12] conjugated microporous polymers (CMPs),[13,14] and amine-modified mesoporous silica.[15] Compared to these CO_2 adsorbents, the carbon-based materials displayed a relatively high CO_2 adsorption capacity and selectivity over a wide range of operation conditions.[16,17] Because of their high specific surface area, uniform and narrow pore size distribution, and adjustable surface properties, carbon materials have also been used in many other applications, including supercapacitor[18,19] and wastewater treatment.[20,21]

In order to enhance adsorbent performance of adsorption capacity and selectivity, doping heteroatoms to the adsorbent surface/internal is a very efficient method; thus, multiple functional groups have been investigated. The amine groups are commonly chosen due to their significant improvement in gas uptake and selective adsorption ability.[22−24] Other candidates are tested as well such as borane[25,26] and sulfur.[1] In 2011, Jiang et al.[27] computationally designed new porous aromatic frameworks (PAFs) by introducing polar organic groups to the biphenyl unit and then investigated their separating power toward CO_2 by using grand canonical Monte Carol (GCMC) simulations. They found that tetrahydrofuran-like ether-functionalized PAF-1 had the highest CO_2 adsorption capacity and selectivities. Torrisi et al.[28] predicted that −COOH and −OH substituted MIL-53(lp) showed the best CO_2/CH_4 selectivity when compared to original and other functionalized MIL-53(lp).

Abundant natural monomer resources,[29,30] MOFs,[31] and industrial wastes[32] have provided a lot of variability for making carbon materials. Recently, polymers have attracted a special interest for practical applications as pyrolysis precursors of carbon material. Salasubramanian et al.[33] used polythiophene (PTh) as an electrocatalyst in 2011. In 2012, Chandra et al.[24] demonstrated that an N-doped carbon prepared by chemical activation of polypyrole exhibited a high CO_2 adsorption

Received: July 2, 2015
Revised: August 7, 2015
Published: August 10, 2015

DOI: 10.1021/acs.langmuir.5b02390
Langmuir 2015, 31, 9845−9852

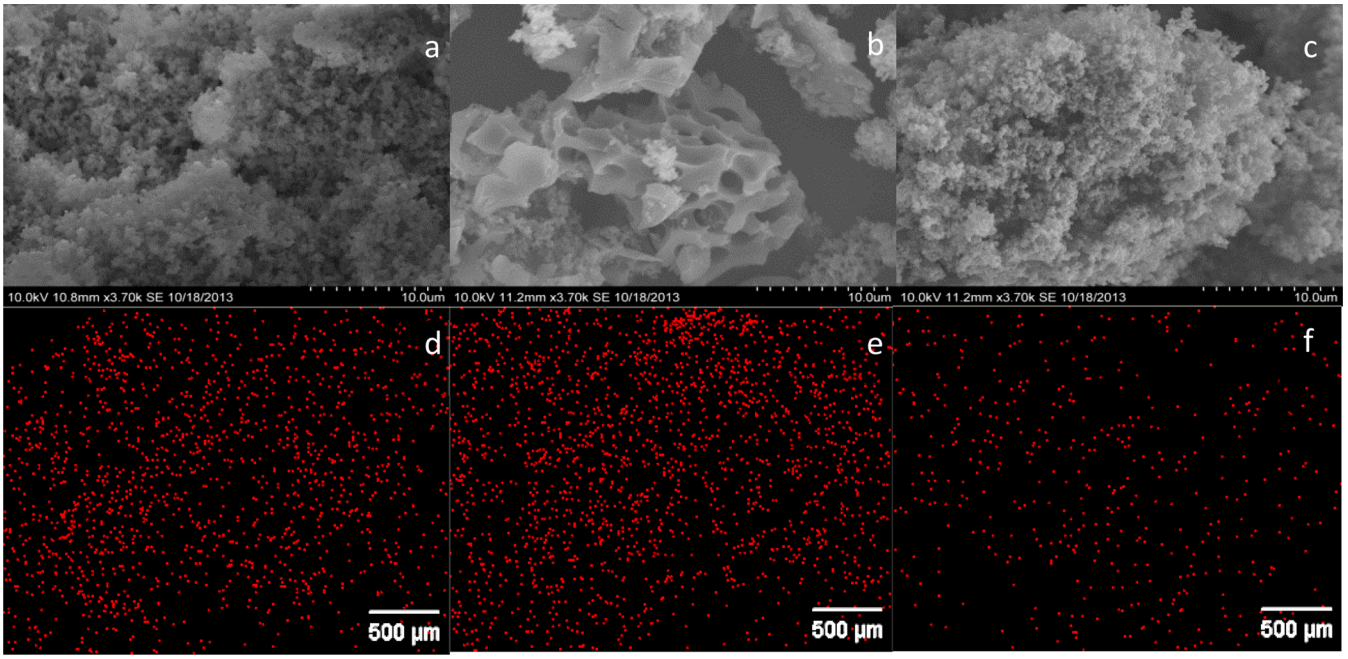

Figure 1. SEM images of (a) original polyfuran, (b) PF-600 KOH, (c) PF-600 $ZnCl_2$, (d) original polyfuran EDS mapping for O, (e) PF-600 KOH EDS mapping for O, and (f) PF-600 ZnCl2 EDS mapping for O.

capacity of 4.3 mmol g^{-1} at 298 K and 1 bar. In 2013, Kim and co-workers[1] reported a few new polythiophene-based carbon materials produced by KOH activation of a reduced-graphene-oxide/PTh material. These carbons displayed a high CO_2 adsorption capacity of 4.5 mmol g^{-1} at 298 K and 1 bar. The objective of this work is to synthesize, characterize, and evaluate a serial of O-doped microporous carbon adsorbents for improved performance in capturing CO_2 from flue gas, biogas upgrading, and methane storage.

2. EXPERIMENTS AND METHODS

An established synthesis method as described in a published report[34] was used for preparing polyfuran. To synthesize polyfuran, 3 g of furan was dispersed in 50 mL of dichloroethane (DCE) at RT using sonication. 8 g of $FeCl_3$ dissolved in 50 mL of DCE was added to this solution. The resulting solution was stirred and allowed to polymerize for 24 h at room temperature. After polymerization, 100 mL of methanol was added, and the final mixture was filtered. The obtained brown precipitate was washed with 500 mL of methanol and 500 mL of deionized water (DI) water. The precipitate was then resuspended in 100 mL of 1 M HCl at room temperature for 3 h. The solution was filtered, and the precipitate was washed with DI water until neutral pH was observed. Finally, the PF material was dried at 80 °C for 24 h in a vacuum.

The chemical activation of polyfuran (PF) was carried out using a 1:1 ratio of PF and potassium hydroxide or zinc chloride. Typically, 1.5 g of PF and the same weight of KOH or $ZnCl_2$ were added to a molar and then grounded to a uniform mixture. Pyrolysis procedural was achieved by heating the mixture for 1 h in a tube furnace under a N_2 atmosphere at two different temperatures (600 and 800 °C). The heating rate was 3 °C min^{-1}. After activation, the product was washed with 8% HCl until neutral pH was observed and then washed with 500 mL of DI water. The final precipitate was dried under vacuum at 80 °C for 24 h.

The XRD pattern was recorded using a Rigaku Miniflex-II X-ray diffractometer with Cu Kα (λ = 1.5406 Å) radiation, 30 kV/15 mA current, and kβ filter. A step scan with an increment of 0.02° in 2θ and a scan rate of 1°/min were employed to obtain the high-resolution patterns. Fourier transformed infrared (FT-IR) spectra were recorded with a PerkinElmer FTIR. Scanning electron microscopy (SEM) images and EDS mapping of the materials were taken using a SEM S-3400NII equipped with energy-dispersive X-ray analysis (EDS). Transmission electron microscopy (TEM) images were taken by a Hitachi H-7650. Raman spectra were collected using a Reinshaw Raman microscope with 632.8 nm (1.96 eV) laser excitation. The TGA data were collected in PerkinElmer thermogravimetric analyzer from 25 to 900 °C under a nitrogen flow (~100 mL/min), and the heating rate was 10 °C min^{-1}.

The adsorption isotherms of CO_2, CH_4, and N_2 at three temperatures (273, 298, and 323 K) and gas pressure up to 800 mmHg were measured volumetrically in the Micromeritics ASAP 2020 adsorption apparatus. All temperatures were achieved by using a Dewar with a circulating jacket connected to a thermostatic bath with a precision of ±0.01 °C. The degas procedure was repeated in all samples before measurements at 150 °C for 24 h. Ultrahigh purity grade CO_2, CH_4, N_2, and He from Matheson Co. were used as received. The BET (Brunauer–Emmett–Teller) surface area was calculated at 0.05–0.3 relative pressures, and pore size distributions were calculated using NLDFT (nonlocal density functional theory) from N_2 adsorption–desorption isotherms measured at 77 K.

3. RESULTS AND DISCUSSION

3.1. Material Synthesis and Characterization. The polyfuran carbon precursors were synthesized by the polymerization of furan using ferric chloride as a catalyst at room temperature. The polyfuran carbon precursors were then activated using KOH or $ZnCl_2$ as a porogen agent and pyrolyzed at 600 or 800 °C for 1 h. Four polyfuran-derived porous carbon samples, PF-600 KOH, PF-800 KOH, PF-600 $ZnCl_2$, and PF-800 $ZnCl_2$, were obtained with four different combinations of porogen agent and pyrolysis temperature. FT-IR spectra (Figure S1) of these samples were scanned four times at a resolution of 1 cm^{-1}. For all four samples, the bands that appear at approximately 787, 1013, 1498, and 3117 cm^{-1} are contributed to plane C–H aromatic bending, furan ring breathing, C=C stretching in furan ring, and C–H stretching in furan ring, respectively. The remaining peaks in the polyfuran-derived porous carbon samples are attributed to functional groups with the peaks at 1148 and 1250 cm^{-1}

DOI: 10.1021/acs.langmuir.5b02390
Langmuir 2015, 31, 9845–9852

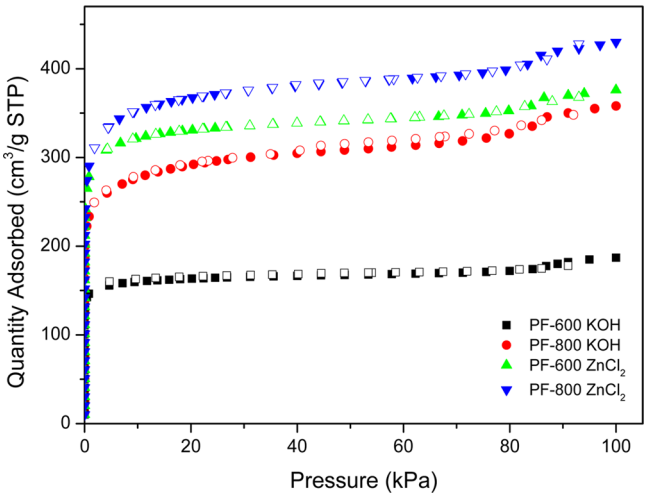

Figure 2. N_2 adsorption (filled symbol)−desorption (open symbol) isotherms of polyfuran-derived carbons at 77 K.

Table 1. Summary of Pore Textural Properties of Original Polyfuran and Polyfuran-Derived Carbons

sample	BET surface area (m^2/g)	Langmuir surface area (m^2/g)	NLDFT pore width (Å)	pore volume (cm^3/g)
original PF	25			
PF-600 KOH	699	849	8.5	0.31
PF-800 KOH	898	1470	9.0	0.53
PF-600 $ZnCl_2$	1006	1567	8.7	0.57
PF-800 $ZnCl_2$	1123	1782	9.2	0.64

corresponding to C−O stretching in furan ring and C−O−C stretching, respectively.

XRD spectra were recorded for all four samples to study the effects of activation temperature and porogen on graphitization in four samples (Figure S2). From the figure, there is no obvious peak using zinc chloride as the porogen agent. Peaks located around 2θ of 29° are found to be present in both PF-600 KOH and PF-800 KOH. The additional peak located around 2θ of 26° is found in PF-800 KOH. These discoveries indicate that graphitization occurs at higher temperature and uses potassium hydroxide as porogen. The TGA results plotted in Figure S3 clearly show a good stability of the polyfuran-derived porous carbon samples at temperatures below 400 °C, which is very important for many practical applications.

Raman spectra of these four samples are shown in Figure S4. The emergence of the D and G bands indicates graphitization occurred in these samples. The increasing D/G intensity ratio in PF KOH samples indicates higher activation temperature, resulting in less ordered carbon. The emergence of these characteristic bands and the downward shift of the G peak of PF-600 KOH and PF-800 KOH compared to PF-600 $ZnCl_2$ and PF-800 $ZnCl_2$ indicate that doped O is more in PF KOH than PF $ZnCl_2$.

The SEM images are shown in Figure 1 and Figure S5. The SEM image of the raw polyfuran is a typical granular morphology (Figure 1a), whereas the SEM images of PF-600 KOH (Figure 1b) and PF-800 KOH (Figure S5b) show the formation of a typical porous carbon structure. The porous surface of PF-600 KOH and PF-800 KOH could be seen by presence of holes on the polyfuran surface after the KOH activation. However, the SEM images of PF-600 $ZnCl_2$ (Figure 1c) and PF-800 $ZnCl_2$ (Figure S5c) show a very similar granular morphology with the original polyfuran. This indicates that $ZnCl_2$ does not change much geochemical surface properties. From the transmission electron microscopy (TEM) figures (Figure S6), apparent oriented multilayer domains and a few indistinguishable graphene sheets stacked in parallel positions were observed in all polyfuran-derived porous carbon samples. Arranged structure with uniform pores was also clearly observed, implying that PFs possess a well ordered 2D hexagonal microstructure with 1D channels. The

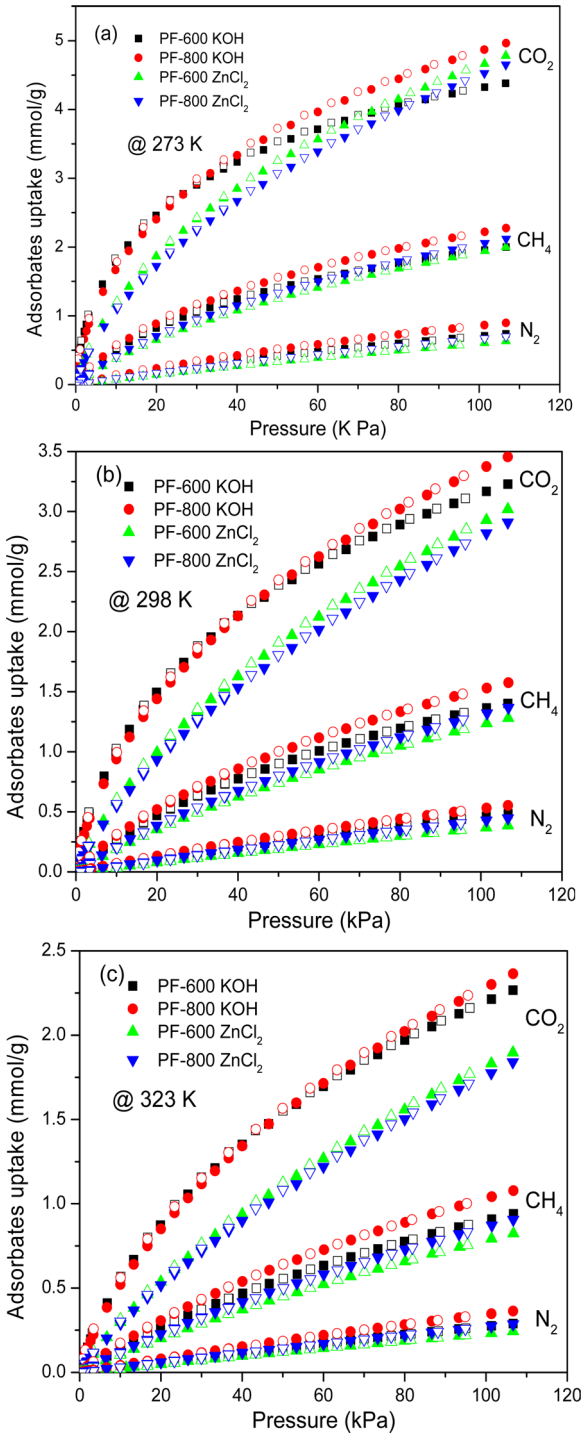

Figure 3. CO_2, N_2, and CH_4 adsorption isotherms for polyfuran-derived carbons at (a) 273, (b) 298, and (c) 323 K and 1 bar (filled symbols: adsorption; open symbols: desorption).

DOI: 10.1021/acs.langmuir.5b02390
Langmuir 2015, 31, 9845−9852

Table 2. Comparison of Adsorption Properties of Polyfuran-Derived Carbons with Other Adsorbents

sample	CO_2 uptake[a] (mmol/g)	CH_4 uptake[b] (mmol/g)	IAST selectivity[c]	ref
PF-600 KOH	3.23	2	41.7 (6.8)	this work
PF-800 KOH	3.46	2.27	27.8 (5.1)	this work
PF-600 $ZnCl_2$	3.02	2	18.5 (3.8)	this work
PF-800 $ZnCl_2$	2.91	2.12	14.1 (3.1)	this work
a-SG7	4.5			1
aNDC-6	4.3			24
NPC-40-800	2.49			40
N-containing carbon monolith	3.13			41
aC-AO2	2.5		20.4 (−)	43
sOMC[d]	3	1.3	12.8 (3.4)	53
silicalite-1	1.63	0.65	9.6 (2.6)	56
MCM-41	1.2	0.3	(−) 4.5	58

[a]Measured at 298 K and 1 bar. [b]Measured at 273 K and 1 bar. [c]CO_2/N_2 (CO_2/CH_4) selectivity measured at 298 K and 1 bar. [d]Measured at 278 K and 1 bar.

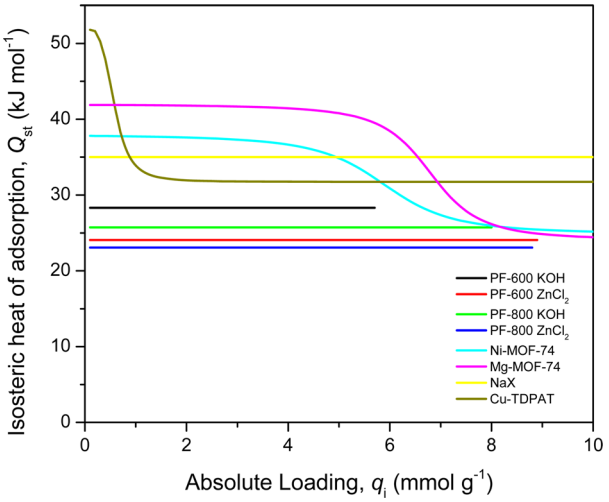

Figure 4. Isosteric heats of adsorption for CO_2 on the polyfuran-derived carbons, MgMOF-74, NiMOF-74 Cu-TDPA, and NaX.

energy-dispersive X-ray spectroscopy (EDS) mapping results of four samples are shown in Figure 1 and Figure S5. A uniform distribution of oxygen on the surface of these samples can be seen. This result shows that O has been successfully doped into the activated materials. From Figure 1e and Figure S5e, we can find that there are no obvious quantitative differences among original polyfuran (Figure 1d), PF-600 KOH, and PF-800 KOH. However, apparent decreases are found in PF-600 $ZnCl_2$ (Figure 1f) and PF-800 $ZnCl_2$ (Figure S5f). These results are consistent with the mechanisms of KOH and $ZnCl_2$ as the activation agents to be discussed in the following section.

3.2. Texture Properties. Figure 2 shows the N_2 adsorption−desorption isotherms of the polyfuran-derived porous carbon adsorbents. The N_2 isotherms of all four samples display a typical type I shape according to IUPAC classification.[35] The steep adsorption in low pressure indicates that all the pores are micropores (<2 nm). This is consistent with the calculated pore size distribution shown in Figure S7.

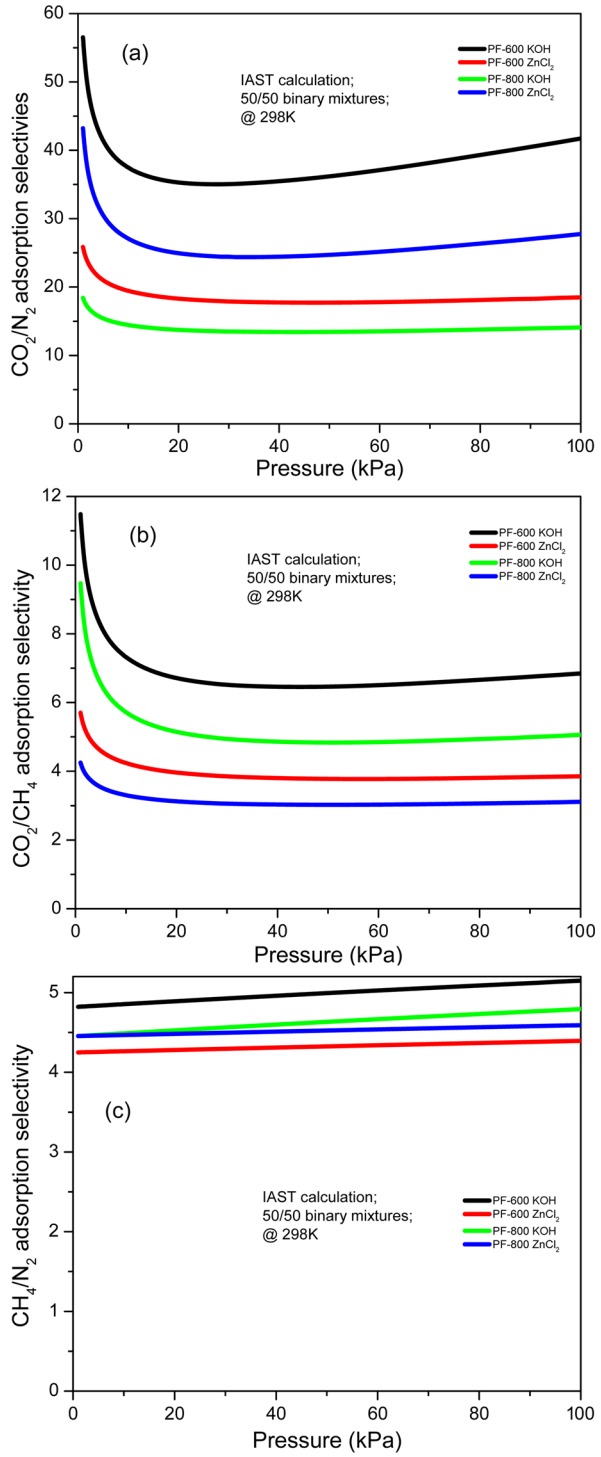

Figure 5. IAST predicted adsorption selectivities for equimolar binary mixtures of (a) CO_2/CH_4, (b) CH_4/N_2, and (c) CO_2/N_2 on PFs at 298 K and 1 atm.

The micropore size distribution and micropore volume were calculated by the nonlocalized density functional theory (NLDFT) method as shown in Table 1. The pore sizes of the polyfuran-derived porous carbons are below 0.9 nm (Table 1), and the molecular size of CO_2 is 0.209 nm. Therefore, polyfuran-derived porous carbon adsorbents are expected to be effective for proficient CO_2 adsorption at an ambient pressure. A lot of efforts have been made to increase the interaction forces between adsorbents and adsorbate molecules, for

DOI: 10.1021/acs.langmuir.5b02390
Langmuir 2015, 31, 9845−9852

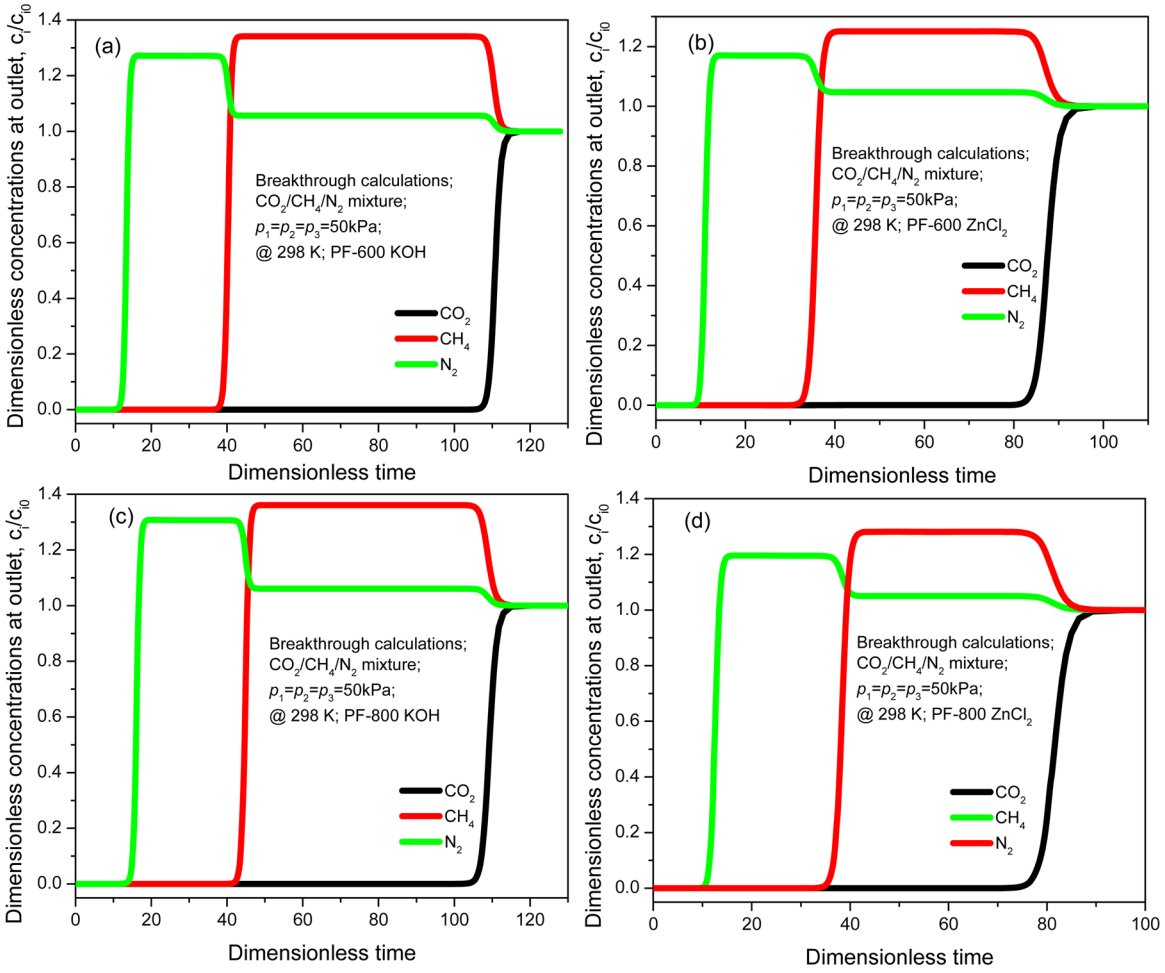

Figure 6. Breakthrough simulation data of (a) PF-600 KOH, (b) PF-600 $ZnCl_2$, (c) PF-800 KOH, and (d) PF-800 $ZnCl_2$ at 298 K and 1 bar for an equimolar $CO_2/CH_4/N_2$ mixture (c_i, the concentration of outlet gas; c_0, the concentration of inlet gas).

example, increasing BET surface area,[5] dosing functional groups,[1,24] and modifying pore structure.[36] Table 1 shows PF-800 $ZnCl_2$ exhibits the largest BET surface area of 1123 m^2 g^{-1}, and largest pore volume of 0.64 cm^3 g^{-1}, as compared to those of other samples. The BET surface areas and pore volumes of KOH activated samples are generally lower than that of $ZnCl_2$ activated samples under the same condition. This is caused by the different mechanisms of porogen. Basically, KOH makes carbon gasification to create pore structure,[37] which preserves most of the O−C functional groups including C═O and C−O−C. While $ZnCl_2$ works as a dehydrate agent,[38] it facilitates the removing of most oxygen from the polyfuran precursors by combining with hydrogen to form H_2O molecules and leaving the carbon skeleton after activation. This is an undesirable feature because it destroys the O−C functional groups, resulting in reduced interaction forces. This mechanism can be proved by the oxygen content as shown in the EDS mapping (Figure 1 and Figure S5). Activation temperature is also a factor affecting the surface properties; a higher temperature leads to a larger surface area and pore volume.

3.3. CO_2, CH_4, and N_2 Adsorption. The single-component adsorption isotherms of CO_2, CH_4, and N_2 measured at 273, 298, and 323 K and gas pressure up to 1 bar are presented in Figure 3 and fitted by the Langmuir−Freundlich model. The calculation details and model parameters are summarized in the Supporting Information (Tables S1−S3). All isotherms show excellent reversibility without a hysteresis, indicating that the adsorbed gas molecules can be easily desorbed by vacuum during the desorption step. The CO_2 adsorption capacity varied with activated temperature and activated agent. The KOH activated polyfuran-derived carbons show an increased CO_2 adsorption capacity from 4.38 to 4.96 mmol g^{-1} when the carbon activating temperature was increased from 600 to 800 °C (Table 2). This is caused by the increased BET surface area and pore volume formed at a higher temperature and the preserved O−C functional groups (by KOH). However, the $ZnCl_2$ activated polyfuran-derived carbons show a decreased CO_2 adsorption capacity from 4.78 to 4.75 mmol g^{-1} when the activation temperature was increased from 600 to 800 °C. This is mainly caused by reduced number of O−C functional groups on carbon adsorbents. Although PF-800 $ZnCl_2$ has a higher BET surface area and pore volume than those of PF-800 KOH and PF-600 $ZnCl_2$, the CO_2 adsorption capacity of PF-800 $ZnCl_2$ is the lowest among these three samples, which strongly suggests that C−O functional groups play a very important role in CO_2 adsorption on the polyfuran-derived carbons, and this discovery is consistent with other literature.[39] Figure 3 also clearly shows KOH activated samples adsorbed more CO_2 than the $ZnCl_2$ activated polyfuran-derived carbons in the low pressure range, due to enhanced interaction force between the C−O functional groups and CO_2 molecules. Among the four

DOI: 10.1021/acs.langmuir.5b02390
Langmuir 2015, 31, 9845−9852

polyfuran-derived carbons, PF-800 KOH has the highest CO_2 adsorption capacity due to the enhanced interaction force, optimal O content, and microporosity of this adsorbent.

PF-800 KOH displays a high adsorption capacity of 4.96 at 273 K and 1 bar, which is one of the best CO_2 adsorbents ever reported. This result is much better than that obtained on a recently reported porous carbon,[40−42] some N-doped carbon materials,[17,41] and another surface-modified porous carbon.[43] Likewise, this result is also comparable to the polypyrrole-based activated carbon[24] and the polythiophene-based activated carbon.[1] Additionally, it should be noted that the KOH activated PFs show a larger CO_2 adsorption at low CO_2 pressures (2.5 and 2.4 mmol g^{-1} at P/P_0 = 0.2 for PF-600 KOH and PF-800 KOH, respectively) than other recently synthesized materials,[1] which could be advantageous for capturing CO_2 from flue gas. One main challenge in capturing CO_2 from flue gas is the low CO_2 partial pressure, whereas the O groups create sufficient active CO_2-adsrobing centers to grab the acidic guest molecules. Therefore, the O-doped porous carbons derived from polyfuran look very promising for capturing CO_2 from flue gas.

Another important feature of the polyfuran-derived carbons is their strong methane adsorption capability. PF-800 KOH shows a very high methane adsorption of 2.27 mmol g^{-1} at 273 K and 1 bar, which is far better than many other adsorbents at similar conditions. Porous polymer materials often exhibit a methane capacity between 0.3 and 1.5 mmol g^{-1} at 273 K and 1 bar.[44−46] Activated carbons often exhibit a methane capacity between 0.8 and 1.5 mmol g^{-1}.[1,5] Based on their outstanding methane adsorption capability, the polyfuran-derived carbons can also be applied in methane storage and natural gas upgrading. Furthermore, nitrogen adsorption isotherm is also shown in Figure 3. Obviously, the N_2 uptake is much lower than CO_2 uptake, only about 1/20th of the CO_2 uptake; this provides a foundation for the good CO_2/N_2 selectivity.

3.4. Isosteric Heat of Adsorption. Moreover, by fitting the CO_2 adsorption isotherms measured at 273, 298, and 323 K and applying a variant of the Clausius−Clapeyron equation, the isosteric adsorption heat was calculated (Supporting Information). The isosteric adsorption heats of CO_2 for all four samples were calculated to lie in 28.3, 25.7, 24.1, and 23.1 kJ mol^{-1} for PF-600 KOH, PF-800 KOH, PF-600 $ZnCl_2$, and PF-800 $ZnCl_2$, respectively (Figure 4). The Q_{st} of CH_4 and N_2 are listed in Table S4. We noted that PF-600 KOH exhibits the highest adsorption heat over all range and PF KOH materials exhibit higher adsorption heat than that of the $ZnCl_2$ activated carbons materials. This is due to O−C functional groups are mostly preserved in lower temperature and using KOH as activated agent. Figure 4 also compares the Q_{st} of the polyfuran-derived carbons with that of Mg-MOF-74,[47] NaX,[47] Cu-TDPAT,[48] and Ni-MOF-74;[49,50] Q_{st} of polyfuran-derived carbons are significantly lower than that of zeolite and MOFs. Those values are even lower than recently reported activated carbon, such as HCM-AC-0[16] and aC-AO2.[43] This implies that the cost of regeneration with polyfuran-derived carbons will be significantly lower than that of other materials, and polyfuran-derived carbons are promising adsorbents in industrial applications.

3.5. Separation of Binary Mixtures. The selectivity of preferential adsorption of component 1 over component 2 in a mixture containing 1 and 2, perhaps in the presence of other components too, can be formally defined as

$$S_{ads} = \frac{q_1/q_2}{p_1/p_2}$$

In the above equation, q_1 and q_2 are the absolute component loadings of the adsorbed phase in the mixture. These component loadings are also termed the uptake capacities. In all the calculations to be presented below, the calculations of q_1 and q_2 are based on the use of the ideal adsorbed solution theory (IAST) of Myers and Prausnitz.[51] The accuracy of the IAST calculations for estimation of the component loadings for several binary mixtures in a wide variety of zeolites and MOFs has been established by comparison with configurational-bias Monte Carlo (CBMC) simulations of mixture adsorption.[52] The CO_2/N_2 IAST selectivity was calculated to be 41.7, 27.8, 18.5, and 14.1 at 298 K and 1 bar for PF-600 KOH, PF-800 KOH, PF-600 $ZnCl_2$, and PF-800 $ZnCl_2$, respectively. It is quite clear that PF-600 KOH has the best CO_2/N_2 selectivity due to its most preserved O−C functional groups, which can be proved by the adsorption heat and EDS mapping. These values are significantly higher than other activated carbons, such as ordered mesoporous carbon (∼11.33),[53] MIL-47(v) (∼9),[54] and N-doped hierarchical carbons (∼8.4)[55] at 298 K and 1 atm. The CO_2/CH_4 IAST selectivity was calculated to be 6.8, 5.1, 3.8, and 3.1 at 298 K and 1 bar for PF-600 KOH, PF-800 KOH, PF-600 $ZnCl_2$, and PF-800 $ZnCl_2$, respectively. These values are superior to the most existing adsorbents at the same condition, such as silicalite-1 (∼2.6),[56] SBA-15 (∼5.5),[57] and MCM-41 (∼5.5).[58] The highest CH_4/N_2 selectivity of 5.1 was obtained by PF-600 KOH at 298 K and 1 bar as well. Those comparisons indicate N-ACs are promising adsorbents in flue gas and natural gas processing.

3.6. Transient Breakthrough Simulations. Separations using porous adsorbents are usually conducted in the fixed bed units; in such cases the separation performance is dictated by a combination of adsorption selectivity and uptake capacity. For a proper evaluation of the performance of fixed bed adsorbers it is necessary to carry out transient breakthrough simulations as described in the literature.[59,60] We therefore performed transient breakthrough simulations for separation of $CO_2/CH_4/N_2$ gas mixtures on the polyfuran-derived carbons. The methodology details and movies using the adsorption cycle isotherms fits are provided in the Supporting Information; the methodology used has been verified to be of good accuracy.[61] Figure 6 compares $CO_2/CH_4/N_2$ mixture breakthrough characteristics as a function of the dimensionless time, $\tau = tu/L\varepsilon$. For all three polyfuran-derived carbons the sequence of breakthroughs is N_2, CH_4, and CO_2; this is dictated by the hierarchy of adsorption strengths. CO_2 molecules are strongly adsorbed by the polyfuran-derived carbons, which elutes last in the sequence. The longest retention time obtained on PF-600 KOH, and this material has the best separation performance due to its good CO_2 capacity and highest CO_2/N_2 and CO_2/CH_4 adsorption selectivities. We noted that there is a time interval that we can get pure CH_4 or N_2 using the polyfuran-derived carbons. We compare PFs with ZIF-7 using breakthrough simulation under the same condition, shown in Figure S9. The CO_2 and CH_4 adsorption data of ZIF-7 are from one recently published paper by our group,[62] and the N_2 adsorption is obtained from a US Patent.[63] It is worth to note that the time intervals between two adsorbates are much shorter compared to polyfuran-derived carbons. This implies that polyfuran-derived carbons have a higher equilibrium separation ability of $CO_2/CH_4/N_2$ than ZIF-7.

DOI: 10.1021/acs.langmuir.5b02390
Langmuir 2015, 31, 9845−9852

4. CONCLUSION

Oxygen-doped microporous carbon materials were successfully synthesized via a chemical activation of a polyfuran material using KOH and $ZnCl_2$ as the progen agents. Compared the two progens, KOH shows more advantages than $ZnCl_2$, such as preserving more O−C functional groups and narrower pore size distribution. For the activation temperature, higher activation temperature could create a larger specific surface area and larger pore volume. However, higher action temperature could cause a larger loss of the functional groups. The CO_2 and CH_4 adsorption capacities are up to 4.96 and 2.27 mmol g^{-1} for PF-800 KOH at 273 K and 1 bar. EDS images and FI-IR curves show that oxygen was successfully doped on the carbon surface. SEM images show different surface properties were obtained using different activated agents. Indeed, KOH activated samples show a high CO_2 adsorption at low pressures, up to 2.5 mmol g^{-1} at P/P_0 of 0.2, which explains why the PF materials displayed a very impressive CO_2/N_2 (41.7) and CO_2/CH_4 (6.8) adsorption separation selectivity. Transient breakthrough simulation was conducted to confirm the potentials of using these carbons in industrial applications. These unique features make the polyfuran-derived carbons very promising adsorbents for CO_2 capture from flue gas, biogas upgrading, and CH_4 storage.

■ ASSOCIATED CONTENT

Supporting Information

The Supporting Information is available free of charge on the ACS Publications website at DOI: 10.1021/acs.langmuir.5b02390.

Figures S1−S8 and Tables S1−S4 (PDF)

■ AUTHOR INFORMATION

Corresponding Author

*Tel +1-575-646-4346; Fax +1-575-646-7706; e-mail sdeng@nmsu.edu (S.D.).

Notes

The authors declare no competing financial interest.

■ ACKNOWLEDGMENTS

This project was partially supported by U.S. National Aeronautics and Space Administration (New Mexico Space Grant), U.S. National Science Foundation (EEC 1028968), and New Mexico State University Office of Vice President for Research (GREG awards for J.W. and X.W.).

■ REFERENCES

(1) Seema, H.; Kemp, K. C.; Le, N. H.; Park, S.-W.; Chandra, V.; Lee, J. W.; Kim, K. S. Highly selective CO 2 capture by S-doped microporous carbon materials. *Carbon* **2014**, *66*, 320−326.

(2) van Groenigen, K. J.; Osenberg, C. W.; Hungate, B. A. Increased soil emissions of potent greenhouse gases under increased atmospheric CO_2. *Nature* **2011**, *475* (7355), 214−216.

(3) Li, J. R.; Kuppler, R. J.; Zhou, H. C. Selective gas adsorption and separation in metal-organic frameworks. *Chem. Soc. Rev.* **2009**, *38* (5), 1477−1504.

(4) Kim, D. Y.; Lee, H. M.; Min, S. K.; Cho, Y.; Hwang, I. C.; Han, K.; Kim, J. Y.; Kim, K. S. CO_2 Capturing Mechanism in Aqueous Ammonia: NH3-Driven Decomposition-Recombination Pathway. *J. Phys. Chem. Lett.* **2011**, *2* (7), 689−694.

(5) Ben, T.; Li, Y. Q.; Zhu, L. K.; Zhang, D. L.; Cao, D. P.; Xiang, Z. H.; Yao, X. D.; Qiu, S. L. Selective adsorption of carbon dioxide by carbonized porous aromatic framework (PAF). *Energy Environ. Sci.* **2012**, *5* (8), 8370−8376.

(6) Casco, M. E.; Martinez-Escandell, M.; Silvestre-Albero, J.; Rodriguez-Reinoso, F. Effect of the porous structure in carbon materials for CO_2 capture at atmospheric and high-pressure. *Carbon* **2014**, *67*, 230−235.

(7) Liu, Q. L.; Pham, T.; Porosoff, M. D.; Lobo, R. F. ZK-5: A CO_2-Selective Zeolite with High Working Capacity at Ambient Temperature and Pressure. *ChemSusChem* **2012**, *5* (11), 2237−2242.

(8) Chen, Y. F.; Jiang, J. W. A Bio-Metal-Organic Framework for Highly Selective CO_2 Capture: A Molecular Simulation Study. *ChemSusChem* **2010**, *3* (8), 982−988.

(9) Ghanem, B. S.; Msayib, K. J.; McKeown, N. B.; Harris, K. D. M.; Pan, Z.; Budd, P. M.; Butler, A.; Selbie, J.; Book, D.; Walton, A. A triptycene-based polymer of intrinsic microposity that displays enhanced surface area and hydrogen adsorption. *Chem. Commun.* **2007**, *1*, 67−69.

(10) McKeown, N. B.; Ghanem, B. S.; Msayib, K. J.; Carta, M.; Budd, P. M.; Selbie, J. D. Polymers of intrinsic microporosity (PIMs): Multifunctional organic materials. *Abstr. Pap. Am. Chem. Soc.* **2007**, *234*.

(11) Wood, C. D.; Tan, B.; Trewin, A.; Su, F.; Rosseinsky, M. J.; Bradshaw, D.; Sun, Y.; Zhou, L.; Cooper, A. I. Microporous organic polymers for methane storage. *Adv. Mater.* **2008**, *20* (10), 1916−1921.

(12) Wang, J.; Huang, J. H.; Wu, X. F.; Yuan, B.; Sun, Y. Q.; Zeng, Z. L.; Deng, S. G. Effect of nitrogen group on selective separation of CO_2/N-2 in porous polystyrene. *Chem. Eng. J.* **2014**, *256*, 390−397.

(13) Neti, V. S. P. K.; Wang, J.; Deng, S.; Echegoyen, L. Selective CO 2 adsorption in a porphyrin polymer with benzimidazole linkages. *RSC Adv.* **2015**, *5* (15), 10960−10963.

(14) Neti, V. S. P. K.; Wang, J.; Deng, S.; Echegoyen, L. High and selective CO 2 adsorption by a phthalocyanine nanoporous polymer. *J. Mater. Chem. A* **2015**, *3* (19), 10284−10288.

(15) Serna-Guerrero, R.; Da'na, E.; Sayari, A. New Insights into the Interactions of CO(2) with Amine-Functionalized Silica. *Ind. Eng. Chem. Res.* **2008**, *47* (23), 9406−9412.

(16) Qian, D.; Lei, C.; Wang, E. M.; Li, W. C.; Lu, A. H. A Method for Creating Microporous Carbon Materials with Excellent CO_2-Adsorption Capacity and Selectivity. *ChemSusChem* **2014**, *7* (1), 291−298.

(17) Wang, J.; Krishna, R.; Yang, J.; Dandamudi, K. P. R.; Deng, S. Nitrogen-doped Porous Carbons for Highly Selective CO 2 Capture from Flue Gases and Natural Gas Upgrading. *Mater. Today Commun.* **2015**, *4*, 156.

(18) Yuan, G.-h.; Jiang, Z.-h.; Aramata, A.; Gao, Y.-z. Electrochemical behavior of activated-carbon capacitor material loaded with nickel oxide. *Carbon* **2005**, *43* (14), 2913−2917.

(19) Sato, Y.; Yomogida, K.; Nanaumi, T.; Kobayakawa, K.; Ohsawa, Y.; Kawai, M. Electrochemical Behavior of Activated-Carbon Capacitor Materials Loaded with Ruthenium Oxide. *Electrochem. Solid-State Lett.* **2000**, *3* (3), 113−116.

(20) Matsumoto, S.; Ohtaki, A.; Hori, K. Carbon Fiber as an Excellent Support Material for Wastewater Treatment Biofilms. *Environ. Sci. Technol.* **2012**, *46* (18), 10175−10181.

(21) Malik, P. Dye removal from wastewater using activated carbon developed from sawdust: adsorption equilibrium and kinetics. *J. Hazard. Mater.* **2004**, *113* (1), 81−88.

(22) Aijaz, A.; Fujiwara, N.; Xu, Q. From Metal−Organic Framework to Nitrogen-Decorated Nanoporous Carbons: High CO_2 Uptake and Efficient Catalytic Oxygen Reduction. *J. Am. Chem. Soc.* **2014**, *136* (19), 6790−6793.

(23) Liu, R.-L.; Ji, W.-J.; He, T.; Zhang, Z.-Q.; Zhang, J.; Dang, F.-Q. Fabrication of nitrogen-doped hierarchically porous carbons through a hybrid dual-template route for CO 2 capture and haemoperfusion. *Carbon* **2014**, *76*, 84−95.

(24) Chandra, V.; Yu, S. U.; Kim, S. H.; Yoon, Y. S.; Kim, D. Y.; Kwon, A. H.; Meyyappan, M.; Kim, K. S. Highly selective CO_2 capture on N-doped carbon produced by chemical activation of polypyrrole

DOI: 10.1021/acs.langmuir.5b02390
Langmuir 2015, 31, 9845−9852

functionalized graphene sheets. *Chem. Commun.* **2012**, *48* (5), 735−737.
(25) Oh, J.; Mo, Y.-H.; Le, V.-D.; Lee, S.; Han, J.; Park, G.; Kim, Y.-H.; Park, S.-E.; Park, S. Borane-modified graphene-based materials as CO 2 adsorbents. *Carbon* **2014**, *79*, 450−456.
(26) Cote, A. P.; Benin, A. I.; Ockwig, N. W.; O'Keeffe, M.; Matzger, A. J.; Yaghi, O. M. Porous, crystalline, covalent organic frameworks. *Science* **2005**, *310* (5751), 1166−1170.
(27) Babarao, R.; Dai, S.; Jiang, D.-e. Functionalizing porous aromatic frameworks with polar organic groups for high-capacity and selective CO_2 separation: A molecular simulation study. *Langmuir* **2011**, *27* (7), 3451−3460.
(28) Torrisi, A.; Bell, R. G.; Mellot-Draznieks, C. Functionalized MOFs for enhanced CO_2 capture. *Cryst. Growth Des.* **2010**, *10* (7), 2839−2841.
(29) Wei, H.; Deng, S.; Hu, B.; Chen, Z.; Wang, B.; Huang, J.; Yu, G. Granular Bamboo-Derived Activated Carbon for High CO_2 Adsorption: The Dominant Role of Narrow Micropores. *ChemSusChem* **2012**, *5* (12), 2354−2360.
(30) Wang, J.; Senkovska, I.; Kaskel, S.; Liu, Q. Chemically activated fungi-based porous carbons for hydrogen storage. *Carbon* **2014**, *75*, 372−380.
(31) Liu, B.; Shioyama, H.; Akita, T.; Xu, Q. Metal-organic framework as a template for porous carbon synthesis. *J. Am. Chem. Soc.* **2008**, *130* (16), 5390−5391.
(32) Wahby, A.; Ramos-Fernández, J. M.; Martínez-Escandell, M.; Sepúlveda-Escribano, A.; Silvestre-Albero, J.; Rodríguez-Reinoso, F. High-Surface-Area Carbon Molecular Sieves for Selective CO_2 Adsorption. *ChemSusChem* **2010**, *3* (8), 974−981.
(33) Giacomini, M. T.; Ticianelli, E. A.; McBreen, J.; Balasubramanian, M. Oxygen reduction on supported platinum/polythiophene electrocatalysts. *J. Electrochem. Soc.* **2001**, *148* (4), A323−A329.
(34) González-Tejera, M.; de la Blanca, E. S.; Carrillo, I. Polyfuran conducting polymers: synthesis, properties, and applications. *Synth. Met.* **2008**, *158* (5), 165−189.
(35) Sing, K. S. W.; Everett, D. H.; Haul, R. A. W.; Moscou, L.; Pierotti, R. A.; Rouquerol, J.; Siemieniewska, T. Reporting Physisorption Data for Gas Solid Systems with Special Reference to the Determination of Surface-Area and Porosity (Recommendations 1984). *Pure Appl. Chem.* **1985**, *57* (4), 603−619.
(36) Lu, W. G.; Yuan, D. Q.; Sculley, J. L.; Zhao, D.; Krishna, R.; Zhou, H. C. Sulfonate-Grafted Porous Polymer Networks for Preferential CO_2 Adsorption at Low Pressure. *J. Am. Chem. Soc.* **2011**, *133* (45), 18126−18129.
(37) Tseng, R. L.; Tseng, S. K. Pore structure and adsorption performance of the KOH-activated carbons prepared from corncob. *J. Colloid Interface Sci.* **2005**, *287* (2), 428−437.
(38) Hu, Z. H.; Vansant, E. F. A new composite adsorbent produced by chemical activation of elutrilithe with zinc chloride. *J. Colloid Interface Sci.* **1995**, *176* (2), 422−431.
(39) Wang, J.; Krishna, R.; Yang, J.; Deng, S. Hydroquinone and Quinone-grafted Porous Carbons for Highly Selective CO_2 Capture from Flue Gases and Natural Gas Upgrading. *Environ. Sci. Technol.* **2015**, *49*, 9364.
(40) Gu, J. M.; Kim, W. S.; Hwang, Y. K.; Huh, S. Template-free synthesis of N-doped porous carbons and their gas sorption properties. *Carbon* **2013**, *56*, 208−217.
(41) Hao, G. P.; Li, W. C.; Qian, D.; Lu, A. H. Rapid Synthesis of Nitrogen-Doped Porous Carbon Monolith for CO_2 Capture. *Adv. Mater.* **2010**, *22* (7), 853−857.
(42) Pevida, C.; Drage, T.; Snape, C. E. Silica-templated melamine−formaldehyde resin derived adsorbents for CO 2 capture. *Carbon* **2008**, *46* (11), 1464−1474.
(43) Mahurin, S. M.; Gorka, J.; Nelson, K. M.; Mayes, R. T.; Dai, S. Enhanced CO_2/N-2 selectivity in amidoxime-modified porous carbon. *Carbon* **2014**, *67*, 457−464.
(44) Mastalerz, M.; Oppel, I. M. Rational Construction of an Extrinsic Porous Molecular Crystal with an Extraordinary High Specific Surface Area. *Angew. Chem., Int. Ed.* **2012**, *51* (21), 5252−5255.
(45) Mohanty, P.; Kull, L. D.; Landskron, K. Porous covalent electron-rich organonitridic frameworks as highly selective sorbents for methane and carbon dioxide. *Nat. Commun.* **2011**, *2*, 401.
(46) Rabbani, M. G.; El-Kaderi, H. M. Template-Free Synthesis of a Highly Porous Benzimidazole-Linked Polymer for CO_2 Capture and H-2 Storage. *Chem. Mater.* **2011**, *23* (7), 1650−1653.
(47) Mason, J. A.; Sumida, K.; Herm, Z. R.; Krishna, R.; Long, J. R. Evaluating metal-organic frameworks for post-combustion carbon dioxide capture via temperature swing adsorption. *Energy Environ. Sci.* **2011**, *4* (8), 3030−3040.
(48) Wu, H. H.; Yao, K. X.; Zhu, Y. H.; Li, B. Y.; Shi, Z.; Krishna, R.; Li, J. Cu-TDPAT, an rht-Type Dual-Functional Metal-Organic Framework Offering Significant Potential for Use in H-2 and Natural Gas Purification Processes Operating at High Pressures. *J. Phys. Chem. C* **2012**, *116* (31), 16609−16618.
(49) Krishna, R.; Long, J. R. Screening Metal-Organic Frameworks by Analysis of Transient Breakthrough of Gas Mixtures in a Fixed Bed Adsorber. *J. Phys. Chem. C* **2011**, *115* (26), 12941−12950.
(50) Krishna, R.; van Baten, J. M. In silico screening of zeolite membranes for CO_2 capture. *J. Membr. Sci.* **2010**, *360* (1−2), 323−333.
(51) Myers, A. L.; Prausnitz, J. M. Thermodynamics of Mixed-Gas Adsorption. *AIChE J.* **1965**, *11* (1), 121.
(52) Krishna, R.; van Baten, J. M. Using molecular simulations for screening of zeolites for separation Of CO_2/CH4 mixtures. *Chem. Eng. J.* **2007**, *133* (1−3), 121−131.
(53) Yuan, B.; Wu, X. F.; Chen, Y. X.; Huang, J. H.; Luo, H. M.; Deng, S. G. Adsorption of CO_2, CH4, and N-2 on Ordered Mesoporous Carbon: Approach for Greenhouse Gases Capture and Biogas Upgrading. *Environ. Sci. Technol.* **2013**, *47* (10), 5474−5480.
(54) Liu, B.; Smit, B. Comparative Molecular Simulation Study of CO_2/N-2 and CH4/N-2 Separation in Zeolites and Metal-Organic Frameworks. *Langmuir* **2009**, *25* (10), 5918−5926.
(55) Gutiérrez, M. C.; Carriazo, D.; Ania, C. O.; Parra, J. B.; Ferrer, M. L.; del Monte, F. Deep eutectic solvents as both precursors and structure directing agents in the synthesis of nitrogen doped hierarchical carbons highly suitable for CO 2 capture. *Energy Environ. Sci.* **2011**, *4* (9), 3535−3544.
(56) Yang, J. F.; Li, J. M.; Wang, W.; Li, L. B.; Li, J. P. Adsorption of CO_2, CH4, and N-2 on 8-, 10-, and 12-Membered Ring Hydrophobic Microporous High-Silica Zeolites: DDR, Silicalite-1, and Beta. *Ind. Eng. Chem. Res.* **2013**, *52* (50), 17856−17864.
(57) Saini, V. K.; Andrade, M.; Pinto, M. L.; Carvalho, A. P.; Pires, J. How the adsorption properties get changed when going from SBA-15 to its CMK-3 carbon replica. *Sep. Purif. Technol.* **2010**, *75* (3), 366−376.
(58) Belmabkhout, Y.; Sayari, A. Adsorption of CO_2 from dry gases on MCM-41 silica at ambient temperature and high pressure. 2: Adsorption of CO_2/N-2, CO_2/CH4 and CO_2/H-2 binary mixtures. *Chem. Eng. Sci.* **2009**, *64* (17), 3729−3735.
(59) Krishna, R.; van Baten, J. M. Investigating the Relative Influences of Molecular Dimensions and Binding Energies on Diffusivities of Guest Species Inside Nanoporous Crystalline Materials. *J. Phys. Chem. C* **2012**, *116* (44), 23556−23568.
(60) Krishna, R. The Maxwell-Stefan description of mixture diffusion in nanoporous crystalline materials. *Microporous Mesoporous Mater.* **2014**, *185*, 30−50.
(61) He, Y. B.; Krishna, R.; Chen, B. L. Metal-organic frameworks with potential for energy-efficient adsorptive separation of light hydrocarbons. *Energy Environ. Sci.* **2012**, *5* (10), 9107−9120.
(62) Wu, X. F.; Shahrak, M. N.; Yuan, B.; Deng, S. G. Synthesis and characterization of zeolitic imidazolate framework ZIF-7 for CO_2 and CH4 separation. *Microporous Mesoporous Mater.* **2014**, *190*, 189−196.
(63) Reyes, S. C.; Ni, Z.; Paur, C. S.; Kortunov, P.; Zengel, J.; Deckman, H. W. Separation of carbon dioxide from nitrogen utilizing zeolitic imidazolate framework materials. Google Patents, 2012.

DOI: 10.1021/acs.langmuir.5b02390
Langmuir 2015, 31, 9845−9852

Supporting Material

Polyfuran Derived Microporous Carbons for Enhanced Adsorption of CO_2 and CH_4

Jun Wang [a], Rajamani Krishna [b] , Xiaofei Wu [a], Yingqiang Sun [a], Shuguang Deng [a] *

[a] Chemical Engineering Department

New Mexico State University

Las Cruces, New Mexico, 88003, USA

[b.] Van't Hoff Institute for Molecular Sciences,

University of Amsterdam,

Science Park 904, 1098 XH Amsterdam, The Netherlands

*Corresponding author: Tel: +1-575-646-4346; Fax: +1-575-646-7706.

E-mail address: sdeng@nmsu.edu

Table of Contents

Chemical reagents and materials

Furan (Sigma Aldrich), Ferric Chloride (Sigma Aldrich), Potassium Hydroxide (90%, flakes, Sigma Aldrich), Zinc Chloride (Sigma Aldrich), Hydrochloric Acid (Sigma Aldrich), Methanol (Sigma Aldrich), Dichlorideethane (99%, Sigma Aldrich), CO2, CH4, N2, and He (99.999%, Matheson Co.) All materials are used as received.

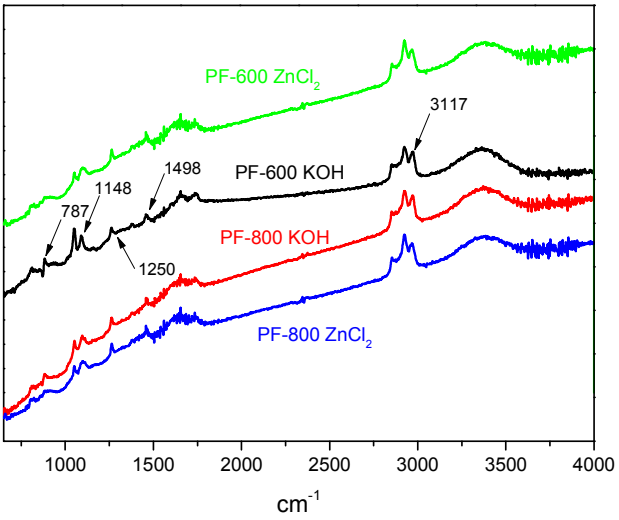

Figure S1. FT-IR spectra of polyfuran-derived porous carbons

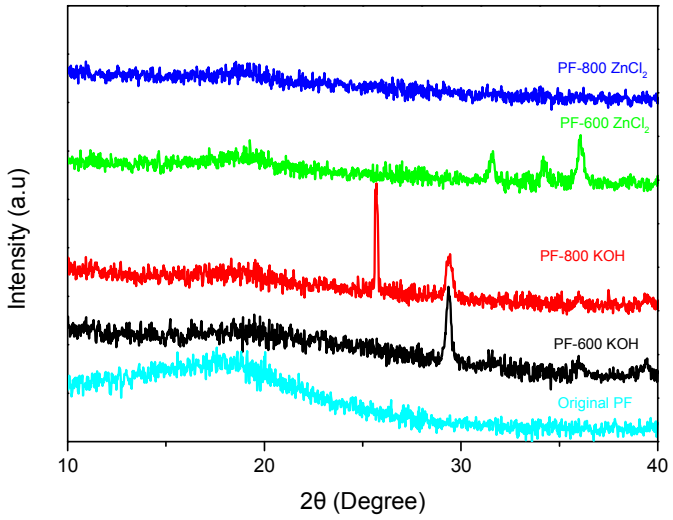

Figure S2. Powder X-ray diffraction patterns of polyfuran and polyfuran-derived porous carbons

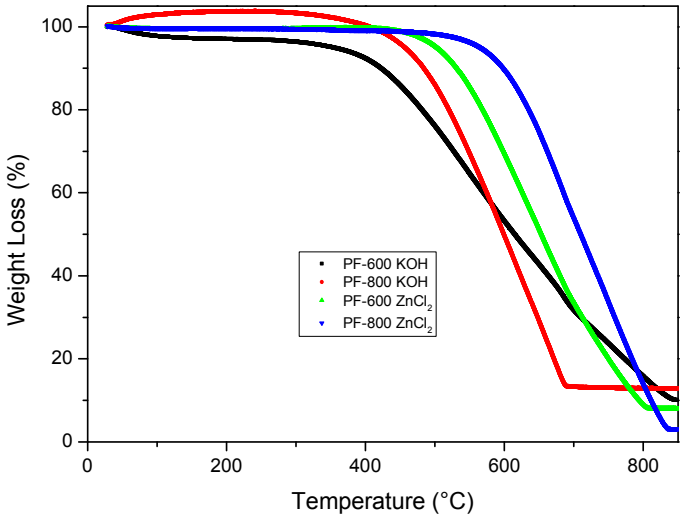

Figure S3. TGA plots of polyfuran-derived porous carbons

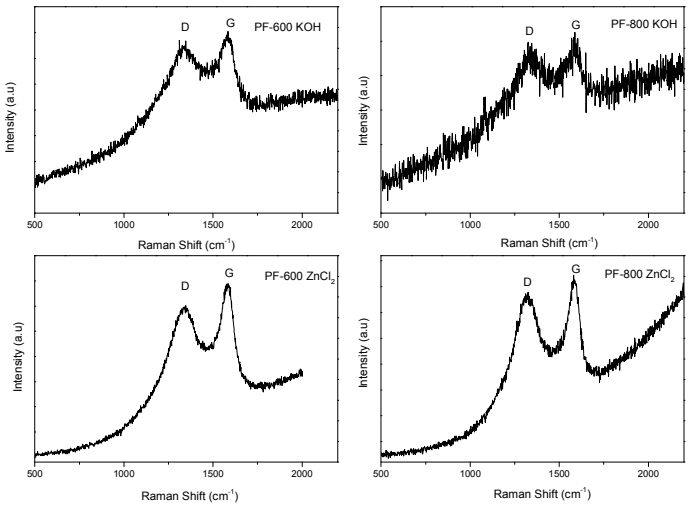

Figure S4. Raman spectra for polyfuran-derived porous carbons

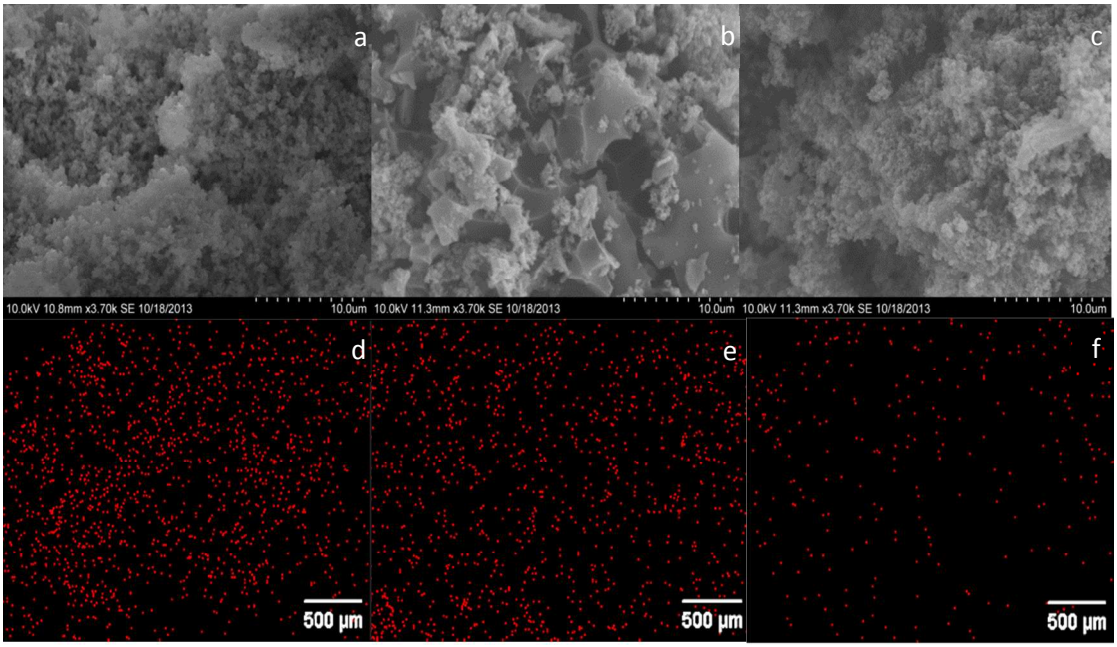

Figure S5. (a) SEM image for original polyfuran, (b) SEM image for PF-800 KOH, (c) SEM image for PF-800 $ZnCl_2$, (d) EDS image for original polyfuran, (e) EDS image for PF-800 KOH, (f) EDS image for PF-800 $ZnCl_2$

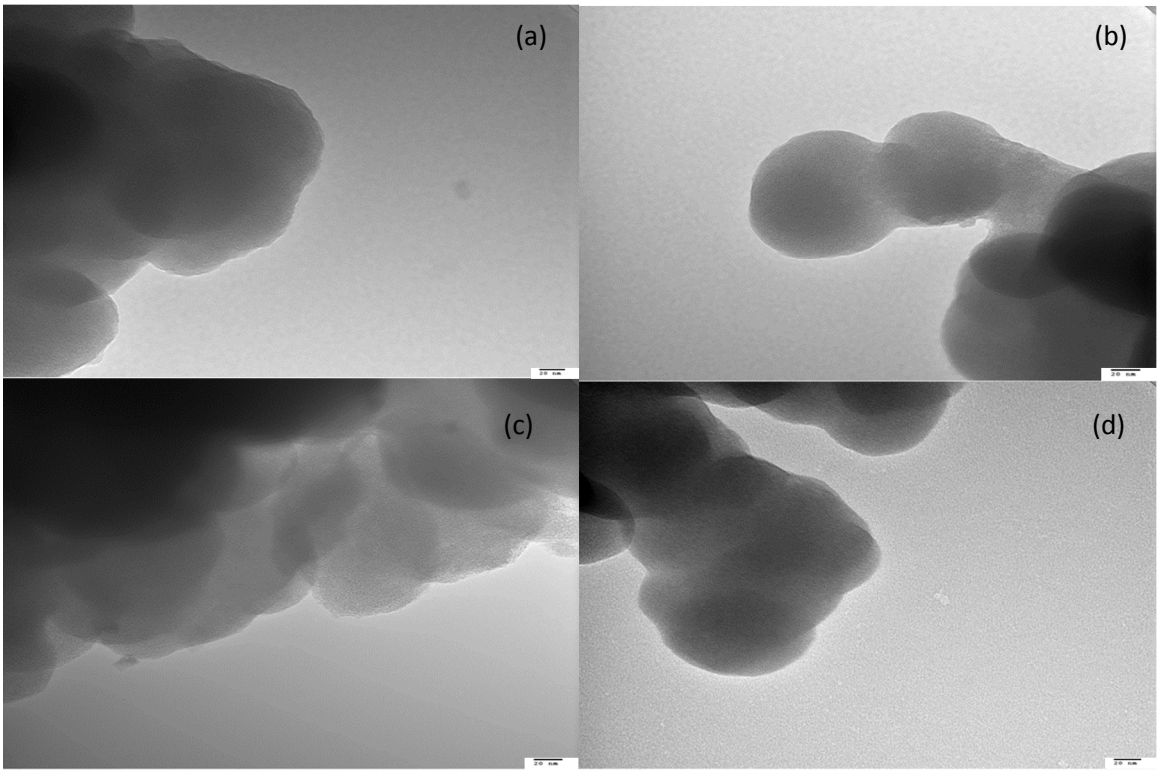

Figure S6. (a) TEM image for PF-600 $ZnCl_2$, (b) PF-600 KOH, (c) PF-800 $ZnCl_2$, (d) PF-800 KOH.

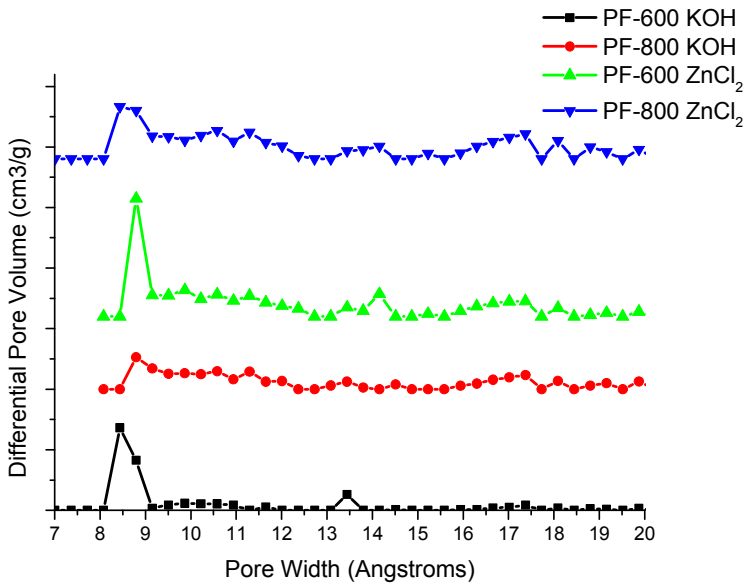

Figure S7. Pore size distribution of polyfuran-derived porous carbons

Fitting of pure component isotherms

The experimentally measured loadings for (a) CO_2, (b) CH_4, and (c) N_2 were measured as a function of the absolute pressure at three different temperatures 273 K, 298 K, and 323 K.

The isotherm data for CO_2 were fitted with the Langmuir-Freundlich model

$$q = q_{sat} \frac{bp^{\nu}}{1 + bp^{\nu}} \tag{1}$$

with T-dependent parameter b

$$b = b_0 \exp\left(\frac{E}{RT}\right) \tag{2}$$

The Langmuir-Freundlich parameters for adsorption of CO_2 are provided in Table 1 for PF-600 KOH, PF-600 $ZnCl_2$, PF-800 KOH, and PF-800 $ZnCl_2$.

The simpler single-site Langmuir model

$$q = q_{sat}\frac{bp}{1+bp}; \quad b = b_0 \exp\left(\frac{E}{RT}\right) \tag{3}$$

was adequate for fitting the isotherm data for CH_4 and N_2; Table 2 and Table 3 provides the *T*-dependent Langmuir parameters for PF-600 KOH, PF-600 $ZnCl_2$, PF-800 KOH, and PF-800 $ZnCl_2$ for CH_4 and N_2, respectively.

Table S5. Langmuir-Freundlich parameters for adsorption of CO_2 in polyfuran-derived porous carbons.

	q_{sat} mol kg^{-1}	b_0 Pa$^{-\nu}$	E kJ mol^{-1}	ν dimensionless
PF-600 KOH	5.8	2.56×10^{-8}	21.8	0.77
PF-600 $ZnCl_2$	9	5.7×10^{-9}	20.7	0.86
PF-800 KOH	8	5.35×10^{-8}	19.3	0.75
PF-800 $ZnCl_2$	8.9	5.13×10^{-9}	20.3	0.88

Table S6. 1-site Langmuir parameters for CH_4 in in polyfuran-derived porous carbons.

	q_{sat} mol kg^{-1}	b_0 Pa^{-1}	E kJ mol^{-1}
PF-600 KOH	2.8	1.62×10^{-9}	21.5
PF-600 $ZnCl_2$	3.8	1.63×10^{-9}	19.8
PF-800 KOH	3.1	2.32×10^{-9}	20.7
PF-800 $ZnCl_2$	3.8	2.06×10^{-9}	19.5

Table S7. 1-site Langmuir parameters for N_2 in polyfuran-derived porous carbons.

	q_{sat} mol kg^{-1}	b_0 Pa^{-1}	E kJ mol^{-1}
PF-600 KOH	2.2	2.74×10^{-9}	16.9
PF-600 $ZnCl_2$	3.1	2.08×10^{-9}	16
PF-800 KOH	2.4	2.45×10^{-9}	17.5
PF-800 $ZnCl_2$	3.1	3.11×10^{-9}	15.4

Isosteric heat of adsorption

The isosteric heat of adsorption, Q_{st}, defined as

$$Q_{st} = RT^2\left(\frac{\partial \ln p}{\partial T}\right)_q$$

were determined using the pure component isotherm fits using the Clausius-Clapeyron equation, where Qst (kJ/mol) is the isosteric heat of adsorption, T (K) is the temperature, p (kPa) is the pressure, R is the gas constant. The values of Q_{st} for CO_2, CH_4, and N_2 are provided in Table S4 of PFs.

Table S8. Isosteric heats of adsorption of CO_2, CH_4 and N_2 in polyfuran-derived porous carbons.

	Q_{st}, CO_2 kJ mol^{-1}	Q_{st}, CH_4 kJ mol^{-1}	Q_{st}, N_2 kJ mol^{-1}
PF-600 KOH	28.31	21.5	16.9
PF-600 $ZnCl_2$	24.07	19.8	16
PF-800 KOH	25.7	20.7	17.5
PF-800 $ZnCl_2$	23.07	19.5	15.4

IAST calculations

The adsorption selectivity for the mixtures CH_4/N_2 and CO_2/CH_4 defined by

$$S_{ads} = \frac{q_1/q_2}{p_1/p_2}$$

were calculated according to IAST model proposed by Myers [1,2]. In above equation, q_1 and q_2 are the absolute component loadings of the adsorbed phase in the mixture. These component loadings are also termed the uptake capacities.

Simulation methodology for transient breakthrough in fixed bed adsorbers

The separation of CO_2/CH_4, CO_2/N_2, and CH_4/N_2 mixtures is commonly carried out in fixed bed adsorbers in which the separation performance is dictated by a combination of three separate factors: (a) adsorption selectivity, (b) uptake capacity, and (c) intra-crystalline diffusivities of guest molecules within the pores. Transient breakthrough simulations are required for a proper evaluation of microporous materials; the simulation methodology used in our work is described in earlier publications [3,4].

In order to evaluate the different OACs, breakthrough calculations were performed taking the following parameter values: inside diameter of tube = 50 mm; bed length, L = 1.8 m; voidage of bed, $\varepsilon = 0.5$; superficial gas velocity, u = 0.05 m/s (at inlet), interstitial velocity, v = 0.1 m/s. The mass of adsorbent packed in the tube is 2 kg; see schematic in Figure S8.

A brief summary of the simulation methodology is presented below.Assuming plug flow of an n-component gas mixture through a fixed bed maintained under isothermal

conditions (see schematic in Figure S8), the partial pressures in the gas phase at any position and instant of time are obtained by solving the following set of partial differential equations for each of the species *i* in the gas mixture [5].

$$\frac{1}{RT}\frac{\partial p_i(t,z)}{\partial t} = -\frac{1}{RT}\frac{\partial\left(v(t,z)\,p_i(t,z)\right)}{\partial z} - \frac{(1-\varepsilon)}{\varepsilon}\rho\frac{\partial \bar{q}_i(t,z)}{\partial t}; \quad i = 1,2,...n \tag{1}$$

In equation (1), t is the time, z is the distance along the adsorber, ρ is the framework density, ε is the bed voidage, v is the interstitial gas velocity, and $\bar{q}_i(t,z)$ is the *spatially averaged* molar loading within the crystallites of radius r_c, monitored at position z, and at time t.

At any time t, during the transient approach to thermodynamic equilibrium, the spatially averaged molar loading within the crystallite r_c is obtained by integration of the radial loading profile

$$\bar{q}_i(t) = \frac{3}{r_c^3}\int_0^{r_c} q_i(r,t)r^2 dr \tag{2}$$

For transient unary uptake within a crystal at any position and time with the fixed bed, the radial distribution of molar loadings, q_i, within a spherical crystallite, of radius r_c, is obtained from a solution of a set of differential equations describing the uptake

$$\frac{\partial q_i(r,t)}{\partial t} = -\frac{1}{\rho}\frac{1}{r^2}\frac{\partial}{\partial r}\left(r^2 N_i\right) \tag{3}$$

The molar flux N_i of component i is described by the simplified version of the Maxwell-Stefan equations in which both correlation effects and thermodynamic coupling effects are considered to be of negligible importance [4]

$$N_i = -\rho Đ_i \frac{\partial q_i}{\partial r} \tag{4}$$

Summing equation (2) over all *n* species in the mixture allows calculation of the *total average* molar loading of the mixture within the crystallite

$$\bar{q}_t(t,z) = \sum_{i=1}^{n} \bar{q}_i(t,z) \tag{5}$$

The *interstitial* gas velocity is related to the *superficial* gas velocity by

$$v = \frac{u}{\varepsilon} \tag{6}$$

In industrial practice, the most common operation uses a step-wise input of mixtures to be separated into an adsorber bed that is initially free of adsorbates, i.e. we have the initial condition

$$t = 0; \quad q_i(0,z) = 0 \tag{7}$$

At time, $t = 0$, the inlet to the adsorber, $z = 0$, is subjected to a step input of the *n*-component gas mixture and this step input is maintained till the end of the adsorption cycle when steady-state conditions are reached.

$$t \geq 0; \quad p_i(0,t) = p_{i0}; \quad u(0,t) = u_0 \tag{8}$$

where u_0 is the superficial gas velocity at the inlet to the adsorber.

The breakthrough characteristics for any component is essentially dictated by two sets of parameters: (a) The characteristic contact time $\frac{L}{v} = \frac{L\varepsilon}{u}$ between the crystallites and the surrounding fluid phase, and (b) $\frac{Đ_i}{r_c^2}$, that reflect the importance of intra-crystalline

diffusion limitations. It is common to use the dimensionless time, $\tau = \frac{tu}{L\varepsilon}$, obtained by dividing the actual time, t, by the characteristic time, $\frac{L\varepsilon}{u}$ when plotting simulated breakthrough curves [3].

If the value of $\frac{Đ_i}{r_c^2}$ is large enough to ensure that intra-crystalline gradients are absent and the entire crystallite particle can be considered to be in thermodynamic equilibrium with the surrounding bulk gas phase at that time t, and position z of the adsorber

$$\bar{q}_i(t,z) = q_i(t,z) \tag{9}$$

The molar loadings at the *outer surface* of the crystallites, i.e. at $r = r_c$, are calculated on the basis of adsorption equilibrium with the bulk gas phase partial pressures p_i at that position z and time t. The adsorption equilibrium can be calculated on the basis of the IAST. The assumption of thermodynamic equilibrium at every position z, and any time t, i.e. invoking Equation (5), generally results in sharp breakthroughs for each component. Sharp breakthroughs are desirable in practice because this would result in high productivity of pure products. Essentially, the influence of intra-crystalline diffusion is to reduce the productivity of pure gases. For all the breakthrough calculations reported in this work, we assume negligible diffusion resistances for all materials and we invoke the simplified Equation (5).

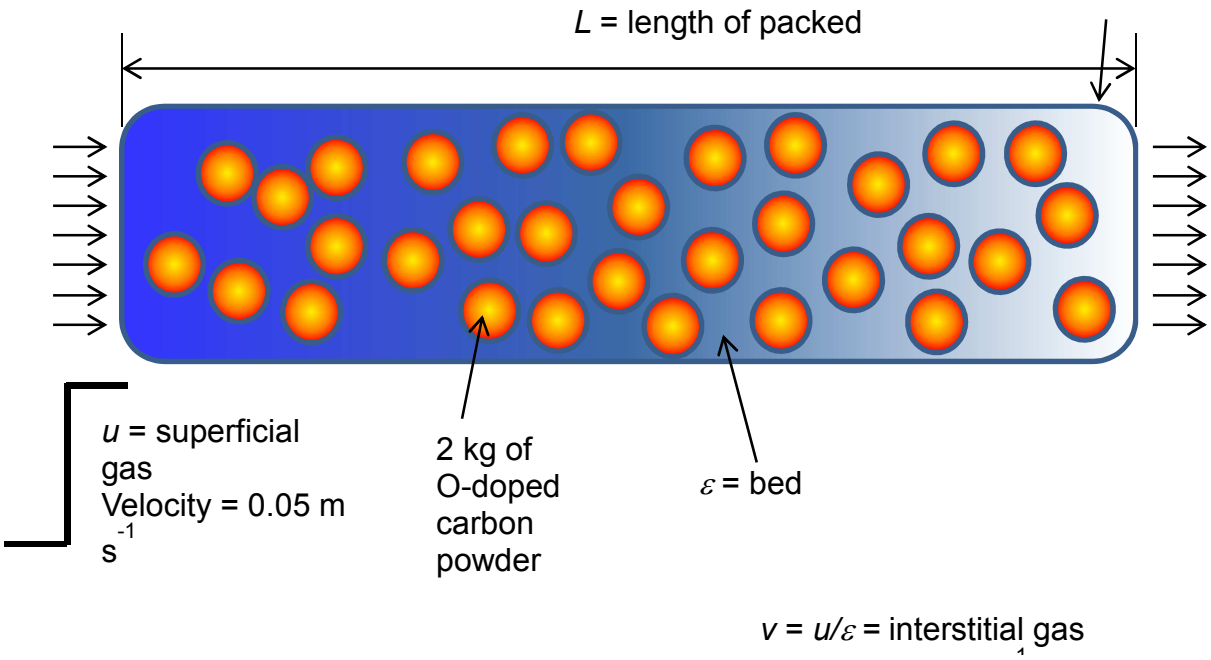

Figure S8. Schematic of the breakthrough apparatus.

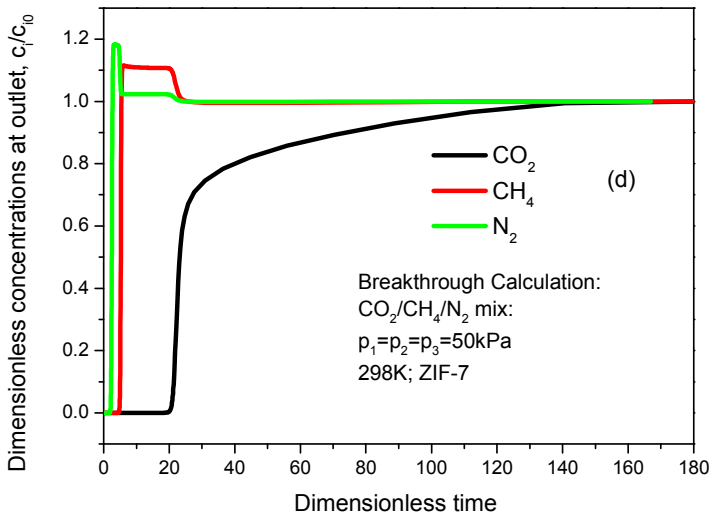

Figure S9. Breakthrough simulation data of ZIF-7 at 298 K and 1 bar for an equimolar $CO_2/CH_4/N_2$ mixture, (c_i, the concentration of outlet gas; c_0, the concentration of inlet gas).

Notation

b	Langmuir-Freundlich constant for species i at adsorption site A, $\mathrm{Pa}^{-\nu_i}$
c_i	molar concentration of species i in gas mixture, mol m^{-3}
c_{i0}	molar concentration of species i in gas mixture at inlet to adsorber, $molm^{-3}$
E	energy parameter, J mol^{-1}
L	length of packed bed adsorber, m
N_i	molar flux of species i, mol m^{-2} s^{-1}
p_i	partial pressure of species i in mixture, Pa
p_t	total system pressure, Pa
q_i	component molar loading of species i, mol kg^{-1}
$\bar{q}_i(t)$	spatially averaged component molar loading of species i, mol kg^{-1}
Q_{st}	isosteric heat of adsorption, J mol^{-1}
r_c	radius of crystallite, m
R	gas constant, 8.314 J mol^{-1} K^{-1}
t	time, s
T	absolute temperature, K
u	superficial gas velocity in packed bed, m s^{-1}
v	interstitial gas velocity in packed bed, m s^{-1}

Greek letters

ε	voidage of packed bed, dimensionless
ρ	framework density, kg m^{-3}
τ	time, dimensionless

Reference

[1]. Myers, A. L.; Prausnitz, J. M. Thermodynamics of mixed gas adsorption, A.I.Ch.E.J. 1965, 11, 121-130.

[2]. Myers AL. Equation of state for adsorption of gases and their mixtures in porous materials. Adsorption. 2003 Mar;9(1):9-16.

[3]. Krishna R, Long JR. Screening metal-organic frameworks by analysis of transient breakthrough of gas mixtures in a fixed bed adsorber. J Phys Chem C. 2011;115:12941-50.

[4]. Krishna R. The Maxwell-Stefan Description of Mixture Diffusion in Nanoporous Crystalline Materials. Microporous Mesoporous Mater. 2014;185:30-50.

[5]. Krishna R, Baur R. Modelling issues in zeolite based separation processes. Sep Purif Technol. 2003;33:213-54.